Materials Transactions, Vol. 47, No. 4 (2006) pp. 1140 to 1144

Wear Characteristics of a Laser Surface Alloyed Al-Mg-Si with Co Alloy Powder

Yao-Chih Chuang[1,*], Shih-Chin Lee[1] and Hsin-Chih Lin[2]

[1]*Department of Materials Science and Engineering, National Cheng Kung University, Tainan, Taiwan, R. O. China*
[2]*Department of Materials Science and Engineering, National Taiwan University, Taipei, Taiwan, R. O. China*

The microstructure and wear resistance of a laser surface alloyed Al-Mg-Si with Co alloy powder were investigated. The experimental results indicate that a porosity-free zone can be generated but some cracks appear after laser surface alloying (LSA). In this investigation, two regions, A (surface region) and B (bottom region), are observed in the pool. Al_9Co_2 particles with a network structure are present in region A and block-like $Al_{13}Co_4$ particles are distributed in region B. The hardness of the LSA specimens is three to nine times higher than that of the Al-matrix. The high hardness of LSA specimens cause them to exhibit excellent sliding wear performance so they have a lower friction coefficient and wear rate. Notably, the critical temperature of the sliding wear resistance of the LSA specimen exceeds that of the Al-matrix by approximately 50 K.

(Received October 27, 2005; Accepted February 27, 2006; Published April 15, 2006)

Keywords: *aluminum-magnesium-silicon alloy, cobalt-based alloy, laser surface alloying, sliding wear*

1. Introduction

Aluminum alloys are known to exhibit two types of sliding wear behaviors, which can be classified as "mild" and "severe", following Archard and Hirst.[1)] Wear characterized by the removal of material in relatively large fragments is defined as severe wear and sliding contact at low loads and low sliding speeds generally causes mild wear. The transition from mild to severe wear of each material corresponded to a temperature range in which the flow strengths and work hardening rates decreased abruptly.[2,3)] Bowden and Tabor[4)] also considered the role of temperature in the wear transition. These researchers also suggested that "strong adhesion" between two surfaces in contact with other occurs at a temperature that lies between 0.4 and 0.5 times the melting temperature of the alloy. In 6061 Al block-on-steel ring wear experiments on dry sliding,[5)] the temperature of the mild to severe wear transition was around 400 K.

Laser surface alloying (LSA) is a relatively newly developed technique of laser surface melting with the simultaneous, controlled addition of alloying elements.[6,7)] Numerous researchers have performed the LSA of Al alloys using various metals and ceramics and they have demonstrated that the surface mechanical/chemical properties of wear,[8–11)] corrosion[12)] and cavitation erosion resistance.[13)] Up to now, the Ni- and Co-based alloys are the most common alloys for enhancing wear resistance. Ni-based alloys are commercially available and frequently used in Al alloys, because of their low melting points and high hardness. When Ni is the main element, the crystal lattice is the same as that of Al, and some intermetallic compounds can be formed by LSA.[14)] However, Co-based alloys perform excellently in high-load and high-temperature sliding on the ferrous alloys. But the microstructure and mechanism on Al alloys with Co-based alloys by LSA have not been known yet.

This investigation studies the microstructure, the hardness and the wear resistance of Co-based alloy using the CO_2 continuous-wave laser technique. The effects of the temperature on the mild and severe wear transitions in Al-Mg-Si alloy and LSA specimens are examined.

Table 1 The chemical compositions of the Co-based alloy (in mass%).

Elements	Co	Cr	W	Si	Fe	C
Co-based alloy (in mass%)	Bal.	30.1	12.6	1.1	3.7	2.4

2. Experimental Procedure

The substrate material was Al-Mg-Si alloy (ASTM 6061 Al alloy) with the following composition (in mass percentages); 1.0%Mg, 0.6%Si, 0.7%Fe, 0.27%Cu, 0.15%Zn, 0.15%Ti and the balance is Al. The wear samples ($\Phi 35 \times 20\,mm^3$) were machined from as-extruded billets. The Co-based alloys are spherical particles with diameters of 70–200 um. Its specific gravity is 8.3, which is higher than the Al-matrix. Table 1 presents the chemical composition of the Co-based alloy.

LSA was conducted using a 5 KW continuous transverse flow CO_2 laser. The diameter of the laser beam was 2.5 mm; its power density was $7.13 \times 10^4\,W/cm^2$, and the laser scanning velocity was 10 mm/s. The surface of the sample was protected by argon gas during LSA. The flow rate of the fixed powders was approximately 2 g/min, as determined by a powder feeding system. The cross-section of the samples was cut perpendicular to the direction of laser scanning. The microstructure was observed and analyzed using a Hitachi S-4200 scanning electron microscope (SEM). The compositions were analyzed using an EDS attached to the SEM with a probe size on the order of 10 nm and resolution of 1 μm. The hardness was measured using a Vickers Hardness Tester with a load of 50 g for 15 s. For each specimen, the average hardness value was calculated from at least five test readings. The sliding wear behavior was investigated using a ring-on-flat wear tester, as displayed in Fig. 1. The testing temperature was controlled precisely between 300 and 550 K. The flat was made from an LSA sample and the counter-body disc was made of SKD61 with the following composition (in mass percentages); 0.39%C, 1.0%Si, 0.4%Mn, 5.2%Cr, 1.4%Mo,

*Graduate Student, National Cheng Kung University. Corresponding author, E-mail: MAXWELL@cubic.mse.ncku.edu.tw

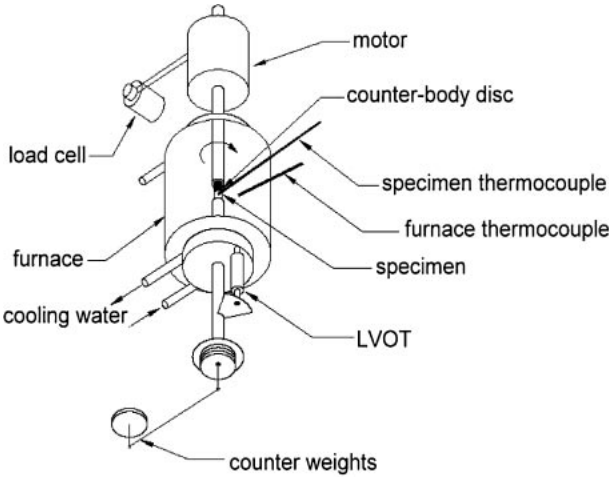

Fig. 1 A schematic representation of ring-on-flat type of wear equipment.

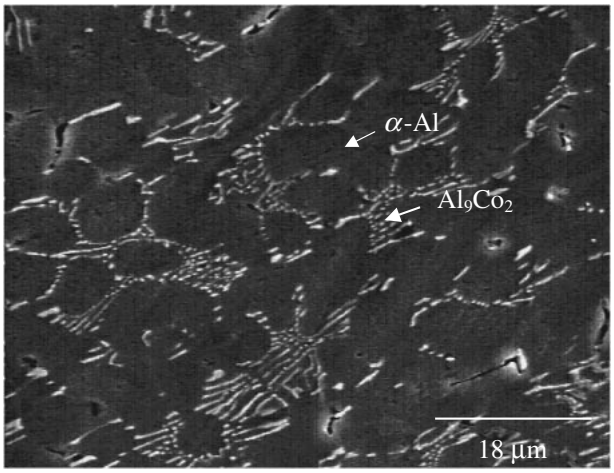

Fig. 3 SEM micrographs of the LSA specimen in the regions A.

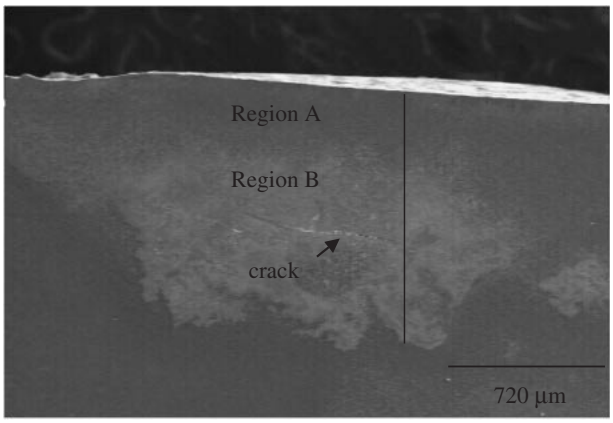

Fig. 2 Photograph of the transverse cross-section of the LSA specimen.

0.8%V and the balance is Fe, which has a hardness of HV630. Before wear testing, about 0.2 mm of the LSA sample was machined off of the surface and then polished to a roughness of $Ra = 0.13\,\mu m$ (center-line-average). The parameters in the sliding wear test were a loading force of 19.6 N, a sliding speed of 0.7 m/s and a sliding distance of 1000 m.

3. Results and Discussion

3.1 Microstructure of an LSA specimen

Figure 2 displays a photograph of the cross-section of a pool of an LSA specimen. We con observe the microstructure distinctly, although the SEM photograph is not very clear. Figure 2 reveals that LSA can form a porosity-free zone, but with some cracks, probably because of the difference of crystal structures between the Co-based alloy and the Al-matrix. Co and Cr are the main elements of a Co-based alloy with HCP and BCC crystal structures, respectively. These alloys differ from the Al-matrix, which has the FCC crystal structure. Subsequently, the Cr element was melted into the pool, increasing the internal friction while reducing the fluidity.[15] The specific gravities of Co and Cr exceed that of the Al-matrix, so they were concentrated at the middle of the bottom of the pool, producing cracks during rapid solidification. The slower solidification in the center of the pool is responsible for higher internal stress there. Therefore, the formation of cracks is reasonable, as presented in Fig. 2.

In this study, two distinct regions, A and B, are clearly observed. A close look at the microstructure of the region A is shown in Fig. 3, which is taken 0.3 mm depth from the surface of the pool in Fig. 2. As shown in Fig. 3, lots of precipitated particles are observed. The chemical constituents of these precipitated particles, magnified and indicated by an arrow tip, are analyzed by EDS. Table 2 presents the results. These precipitated particles are Al_9Co_2 compounds, as indicated by the data in Table 2 and the binary phase diagrams of Al-Co.[16–18] Besides, less Cr is present in region A, but it does not form any compounds. It may be dissolved in the Al-matrix. Figure 4(a) presents the change in the microstructure of region B, which is taken 0.6 mm depth from the surface of the pool in Fig. 2. In this region, large block-like particles of intermetallic compounds and small particles are dispersed around the large block-like particles. Table 2 lists the chemical compositions of the block-like structures and small particles. The data in Table 2 reveal that the block-like structures in Fig. 4(a) are $Al_{13}Co_4$ compounds and the small particles are Al_9Co_2 compounds, the same as in region A.[18] Figure 4(b) presents the needle-like particles of

Table 2 The chemical compositions of the precipitated particles in LSA sample. (in mass%)

Position	Structure	Elements (in mass%)					
		Al	Co	Cr	Mg	Si	W
Region A	Net-work microstructure	Bal.	10.0	0.5	0.6	1.4	0.9
Region B	block-like microstructure	Bal.	34.6	0.7	0.6	0.6	1.4
	Needle-like microstructure	Bal.	0.2	21.5	0.1	0.1	—

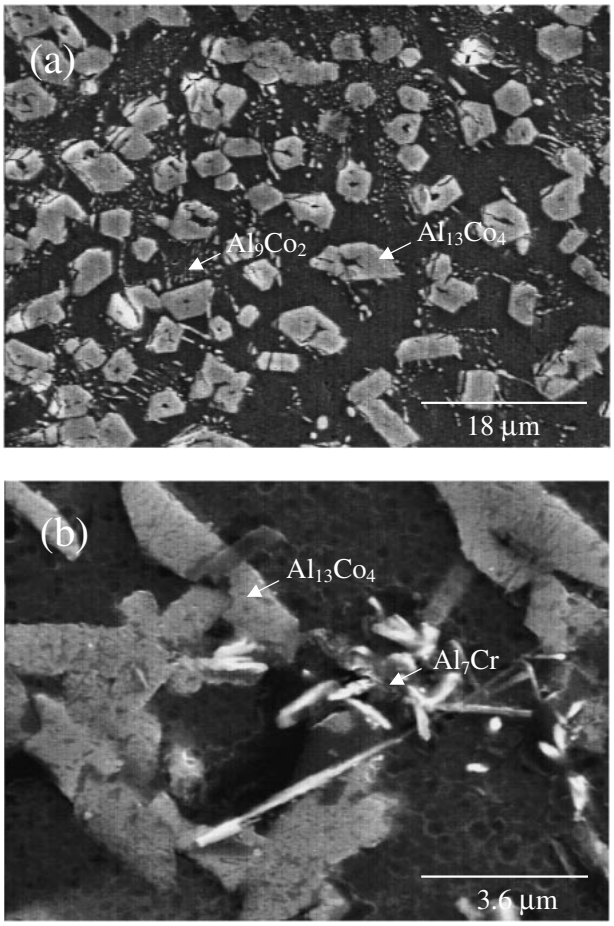

Fig. 4 SEM observation in the region B of the LSA specimen. (a) block-like structures (b) needle-like particles.

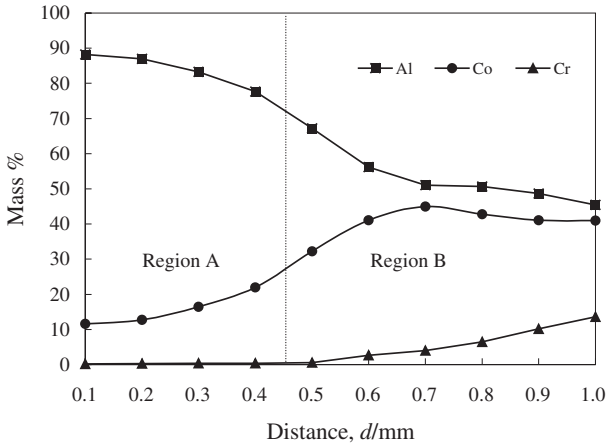

Fig. 5 The distribution of chemical compositions from surface to bottom of the pool in LSA specimen.

Table 3 Hardness of the Al-matrix and LSA specimen.

	Al-matrix	LSA specimen	
Position	All pool	Region A	Region B
Hardness (HV)	60	185	535

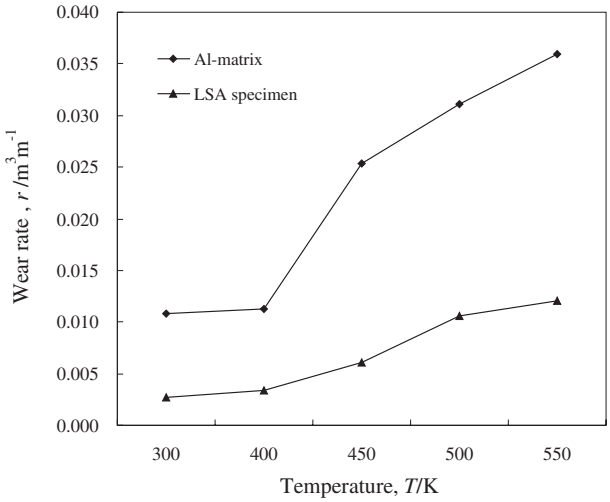

Fig. 6 The curves of wear rate versus temperature for Al-matrix and LSA specimens.

Al_7Cr[19,20] in this region. As mentioned above, the Al_9Co_2 compound is the main structure in the region A because the fast solidification rate lead to less Co element can react with Al-Mg-Si matrix. On the other hand, the more slowly solidification rate in this inner region B was produced $Al_{13}Co_4$ compounds. However, Co and Cr are concentrated at the bottom middle of the pool because they have a larger specific gravity than Al-matrix, as is clearly indicated by a diagram that depicts the change in the concentration profile. Figure 5 shows the concentration profile of the Al, Co and Cr elements at various depths below the surface along the line in Fig. 2. In Fig. 5, Co is dispersed throughout regions A and B, but almost all Cr is concentrated in region B, which is the lower region of the pool. This finding motivates this study of hardness and wear behavior.

3.2 Microhardness

Table 3 presents the hardness of the Al-matrix, region A and region B in the LSA specimen. Regions A and B of the LSA specimen are harder than the Al-matrix, because compounds are present. A comparison of Fig. 5 and Table 3 demonstrates that hardness increases with the Co content. In region A, the hardness slightly exceeds that of the Al-matrix, because region A contains only tiny Al_9Co_2 particles, which can barely influence the hardness. However, region B is obviously harder than the Al-matrix and region A, because it contains larger particles and various Al-Co compounds. In particular, the large quantity of Cr atoms in this region clearly increases its hardness. The hardness of the LSA specimen reaches HV 185 to 535, which is approximately three to nine times that of the Al-matrix (HV 60).

3.3 Wear test

Wear tests were carried out at 300 to 550 K on both Al-matrix and LSA specimens to examine the effect of the temperature on the wear resistance. Figure 6 demonstrates that the LSA specimens have a very low wear rate, which is 4–8 times less than that of the Al matrix at 300 to 550 K. Since the LSA specimens have large quantity of Al_9Co_2 and $Al_{13}Co_4$-reinforced particulates in regions A and B, their hardness was three to nine times higher than that of the Al-

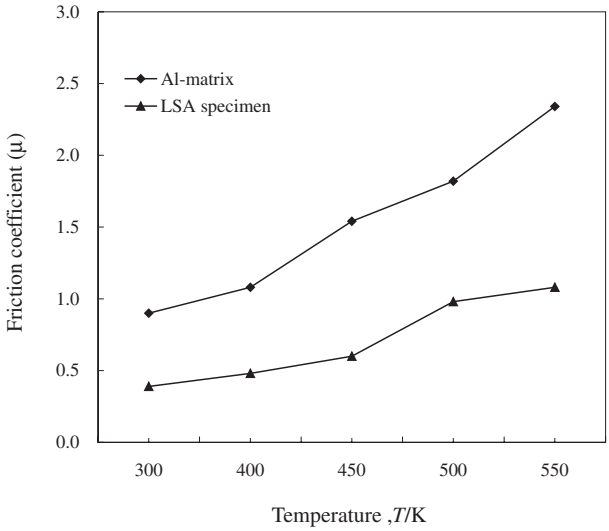

Fig. 7 The curves of friction coefficient versus temperature for the specimens of Al-matrix and LSA specimens.

matrix, so their wear resistance was higher. Therefore, the difference of wear rates for the Al matrix and the LSA specimens are mainly ascribed to their different hardness.[21] Figure 6 also demonstrates that the gradients of wear rate of the Al-matrix versus testing temperature increased rapidly between 400 and 450 K and that of the LSA specimens increased obviously between 450 and 500 K. These findings indicate that the critical temperature of the LSA specimen exceeds that of the Al-matrix by about 50 K. This result is consistent with the viewpoint reported by Martínez *et al.*[22] During the aforementioned sliding wear test, the friction coefficient changed with the temperature. Figure 7 plots the variations in the friction coefficients of the Al-matrix and the LSA specimens from 300 to 550 K. The friction coefficients of both the Al-matrix and the LSA specimens increase with increasing the temperature. The LSA specimens have a lower friction coefficient than the Al-matrix, in which mild wear occurs below 400 K, and severe wear begins when the temperature reaches 450 K. The temperature is 0.4 of the absolute melting temperature.[4] At this temperature, the LSA specimens retain a low friction coefficient until the temperature reaches 500 K. Figure 6 presents a similar phenomenon.

Figures 8(a) to (c) show SEM micrographs of the worn surfaces of LSA specimens that have undergone wear sliding at 400 K, 450 K and 500 K, respectively. As shown in Fig. 8(a), the worn surface is smooth and the ploughing strips are very shallow. This feature is ascribed to the fact that the Al_9Co_2-reinforced particles improve the wear resistance in the mild sliding wear regime. As the temperature is increased to 450 K, the surrounding Al-matrix begins to soften because the critical temperature of sliding wear resistance is between 400 and 450 K (Fig. 6). This characteristic reduces the reinforcement of Al_9Co_2 particles during wear sliding. As presented in Fig. 8(b), the reinforced particles are removed from the edge of the strips and the worn surface exhibits much wear debris. As the testing temperature increases to 500 K, the failure of Al_9Co_2-reinforced particles results in the removal of the worn surface. However, the larger dimensions

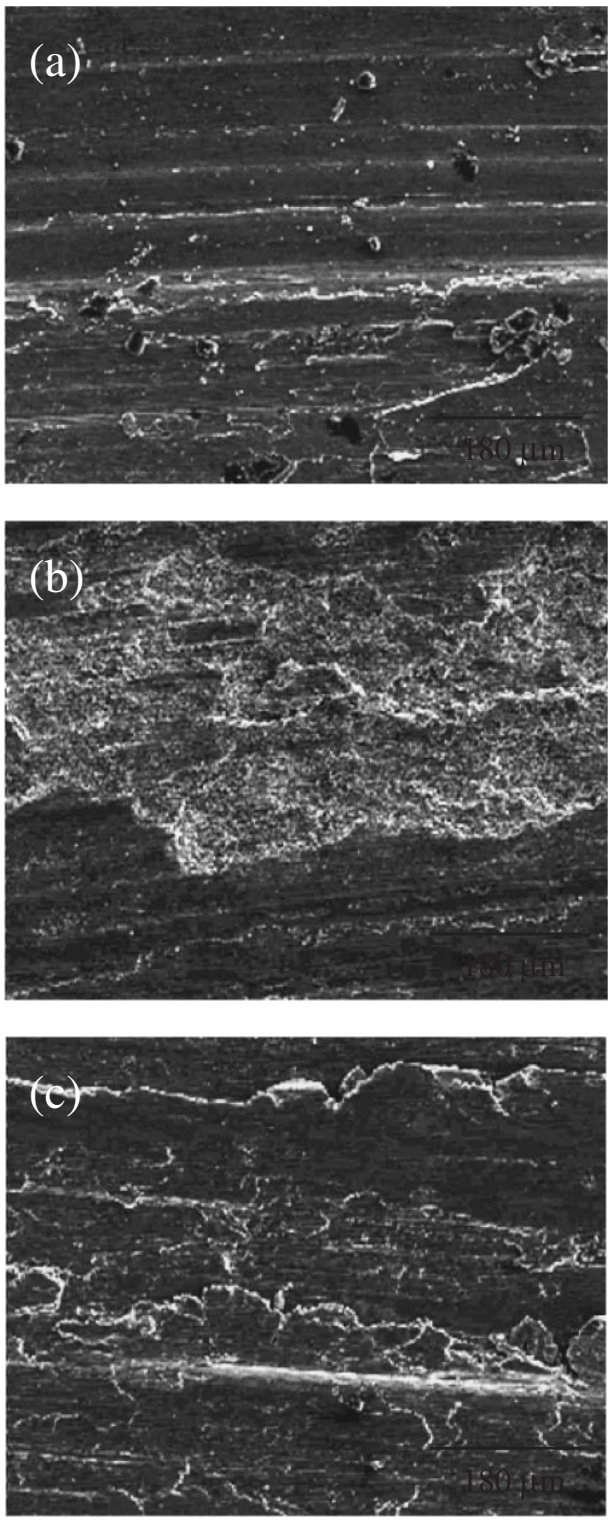

Fig. 8 SEM micrographs of the worn surfaces of LSA specimens with sliding wear at (a) 400 K; (b) 450 K; (c) 500 K.

and hardness of $Al_{13}Co_4$ and Al_7Cr particles in region B increase the wear resistance, even as the temperature rises to 500 K, as displayed in Fig. 8(c). This phenomenon explains why the wear rate of the LSA specimen does not appear to increase from 500 K to 550 K in Fig. 6.

Figures 9(a) and (b) shows the formation of typical wear debris in LSA specimens after the wear test, below and above the critical temperature, respectively. In Fig. 9(a), loose

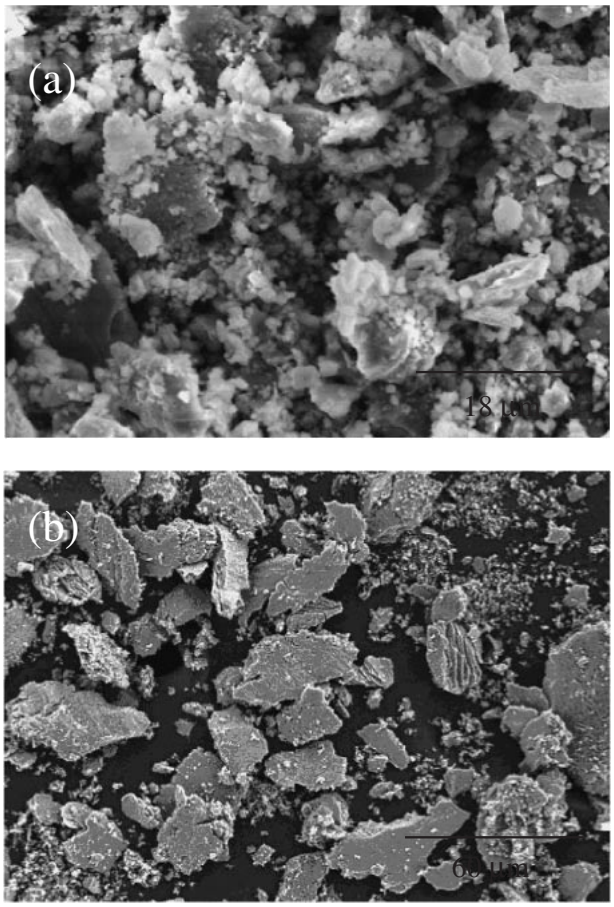

Fig. 9 Morphology of debris of LSA specimens with sliding wear at (a) 400 K; (b) 500 K.

debris with agglomerated small particles with diameters from 1 to 3 μm is observed when tested at 400 K. However, when tested at 500 K, large plate-like debris appeared, as shown in Fig. 9(b). Several observations from the Fig. 8 and Fig. 9 have shown that the critical temperature of LSA specimens is about 450 K.

4. Conclusions

The surface microstructures of the 6061 Al-Mg-Si alloy coated with an LSA Co-based alloy and their sliding wear performance at high temperature were studied. Based on the results of this study, we conclude the following.

(1) Two distinct regions, A and B, are observed in the pool of the LSA specimen. The network structure of the Al_9Co_2 particles is observed in region A, and block-like $Al_{13}Co_4$ and needle-like Al_7Cr particles are distributed in region B.

(2) The LSA specimens are much harder than the Al matrix. The hardness of region A reaches HV 185, which is approximately three times that of the Al-matrix (HV 60). Region B displayed was about nine times harder than the Al-matrix, because the element Cr enhances the hardness.

(3) The LSA specimens have a very low wear rate, which is around 4-8 times less than that of the Al-matrix from 300 to 550 K. Below the critical temperature, the Al_9Co_2-reinforced particles have improved wear resistance in the mild sliding wear regime. Above the critical temperature, the larger dimensions and the greater hardness of the $Al_{13}Co_4$ and Al_7Cr particles in region B improve the wear resistance in the severe sliding wear regime.

(4) The critical temperature associated with the sliding wear resistance of the LSA specimen exceeds that of the Al-matrix by about 50 K.

Acknowledgement

The authors would like to thank the National Science Council of Republic of China, Taiwan, for financially supporting this research under Contract No. NSC89-2216-E-006-078.

REFERENCES

1) J. F. Archard and W. Hirst: Proc. Roy. Soc. A **236** (1956) 397–405.
2) C. Beesley: Wear **171** (1976) 115–122.
3) V. V. Meng: Friction and Wear in Machinery, ASME **14** (1976) 202–211.
4) F. P. Bowden and D. Tabor: *The Friction and Lubrication of Solids*, Part II, (Oxford University Press, London, 1964) p. 97.
5) J. Zhang and A. T. Alpas: Mater. Sci. Eng. A **161** (1993) 273–284.
6) C. T. Kwok, F. T. Cheng, F. T. Cheng and H. C. Man: Surf. Coat. Technol. **107** (1998) 31–40.
7) R. L. Sun, D. Z. Yang, L. X. Guo and S. L. Dong: Surf. Coat. Technol. **132** (2000) 251–255.
8) G. Y. Liang and T. T. Wong: Surf. Coat. Technol. **89** (1997) 121–126.
9) L. J. Yang: Comp. Sci. Technol. **63** (2003) 575–583.
10) Q. Ming, L. C. Lin and Z. D. Chen: Surf. Coat. Technol. **106** (1998) 174–182.
11) Y. B. Liu, J. D. Hu, Z. Y. Cao and P. K. Rohatgi: Wear **206** (1997) 83–86.
12) H. C. Man, S. Zhang, T. M. Yue and F. T. Cheng: Surf. Coat. Technol. **148** (2001) 136–142.
13) W. J. Tomlinson and A. S. Bransden: Wear **185** (1995) 59–65.
14) T. B. Massalski (Ed), *Binary Alloy Phase Diagrams*, (ASM. Metal Park, Ohio, 1 1986) p. 142.
15) G. Z. Zhong: *Laser Processing Technology Handbook*, first ed., (China Measuring, Beijing, 1998) p. 241.
16) T. Gödecke: Z. Metallkde. **62** (1971) 842–847.
17) B. Grushko, R. Wittenberg, K. Bickmann and C. Freiburg: J. Alloys Comp. **233** (1996) 279–287.
18) B. Grushko, D. Holland-Moritz and K. Bickmann: J. Alloys Comp. **236** (1996) 243–252.
19) J. L. Murry, in T. B. Massalski (Ed.), *Binary Alloy Phase Diagrams*, (ASM. International Metal Park, Ohio, 2 1990) p. 138.
20) M. Audier, M. Durand-Charre, E. Laclau and H. klein: J. Alloys Comp. **220** (1995) 225–230.
21) D. Jianxin: Ceram. Inter. **27** (2001) 135–141.
22) M. A. Martínez, A. Martín and J. Llorca: Metall. Mater. **28** (1993) 207–212.